Focusing sub-wavelength grating couplers with low back reflections for rapid prototyping of silicon photonic circuits

Yun Wang,[1,*] **Xu Wang,**[1] **Jonas Flueckiger,**[1] **Han Yun,**[1] **Wei Shi,**[2]
Richard Bojko,[3] **Nicolas A. F. Jaeger,**[1] **and Lukas Chrostowski**[1]

[1]*Department of Electrical and Computer Engineering, University of British Columbia,*
Vancouver, BC, Canada
[2]*Department of Electrical and Computer Engineering, Université Laval, QC, Canada*
[3]*Department of Electrical Engineering, University of Washington, Campus Box 352500,*
Seattle, Washington 98195, USA

[*]*yunw@ece.ubc.ca*

Abstract: We demonstrate fully-etched fiber-waveguide grating couplers with sub-wavelength gratings showing high coupling efficiency as well as low back reflections for both transverse electric (TE) and transverse magnetic (TM) modes. The power reflection coefficients for the TE and TM modes have been significantly suppressed to -16.2 dB and -20.8 dB, respectively. Focusing grating lines have also been used to reduce the footprint of the design. Our sub-wavelength grating couplers for the TE and TM modes show respective measured insertion losses of 4.1 dB and 3.7 dB with 1-dB bandwidths of 30.6 nm (3-dB bandwidth of 52.3 nm) and 47.5 nm (3-dB bandwidth of 81.5 nm), respectively.

References and links

1. D. Vermeulen, S. Selvaraja, P. Verheyen, G. Lepage, W. Bogaerts, P. Absil, D. Van Thourhout, and G. Roelkens, "High-efficiency fiber-to-chip grating couplers realized using an advanced CMOS-compatible silicon-on-insulator platform," Opt. Express **18**, 18278–18283 (2010).
2. A. Mekis, S. Gloeckner, G. Masini, A. Narasimha, T. Pinguet, S. Sahni, and P. De Dobbelaere, "A grating-coupler-enabled CMOS photonics platform," IEEE J. Sel. Top. Quantum Electron. **17**, 597–608 (2011).
3. W. S. Zaoui, A. Kunze, W. Vogel, M. Berroth, J. Butschke, F. Letzkus, and J. Burghartz, "Bridging the gap between optical fibers and silicon photonic integrated circuits," Opt. Express **22**, 1277–1286 (2014).
4. R. Halir, P. Cheben, S. Janz, D.-X. Xu, Í. Molina-Fernández, and J. G. Wangüemert-Pérez, "Waveguide grating coupler with subwavelength microstructures," Opt. Lett. **34**, 1408–1410 (2009).
5. R. Halir, P. Cheben, J. Schmid, R. Ma, D. Bedard, S. Janz, D.-X. Xu, A. Densmore, J. Lapointe, and I. Molina-Fernández, "Continuously apodized fiber-to-chip surface grating coupler with refractive index engineered subwavelength structure," Opt. Lett. **35**, 3243–3245 (2010).
6. X. Xu, H. Subbaraman, J. Covey, D. Kwong, A. Hosseini, and R. T. Chen, "CMOS compatible subwavelength grating couplers for silicon integrated photonics," in *Proceedings of IEEE Photonics Conference* (2012), pp. 350–351.
7. Z. Cheng, X. Chen, C. Y. Wong, K. Xu, and H. K. Tsang, "Apodized focusing subwavelength grating couplers for suspended membrane waveguides," Appl. Phys. Lett. **101**, 101104 (2012).
8. Y. Zhang, T. Baehr-Jones, R. Ding, T. Pinguet, Z. Xuan, and M. Hochberg, "Silicon multi-project wafer platforms for optoelectronic system integration," in *Proceedings of IEEE Group IV Photonics Conference* (2012), pp. 63–65.

9. X. Chen and H. K. Tsang, "Polarization-independent grating couplers for silicon-on-insulator nanophotonic waveguides," Opt. Lett. **36**, 796–798 (2011).
10. Y. Wang, W. Shi, X. Wang, J. Flueckiger, H. Yun, N. A. Jaeger, and L. Chrostowski, "Fully etched grating coupler with low back reflection," in *SPIE Photonics North* (2013), p. 89150U.
11. F. Van Laere, T. Claes, J. Schrauwen, S. Scheerlinck, W. Bogaerts, D. Taillaert, L. O'Faolain, D. Van Thourhout, and R. Baets, "Compact focusing grating couplers for silicon-on-insulator integrated circuits," IEEE Photon. Technol. Lett. **19**, 1919–1921 (2007).
12. http://genisys-gmbh.com/.
13. J. Robinson and Y. Rahmat-Samii, "Particle swarm optimization in electromagnetics," IEEE Trans. Antennas Propag. **52**, 397–407 (2004).
14. X. Chen, K. Xu, Z. Cheng, C. K. Fung, and H. K. Tsang, "Wideband subwavelength gratings for coupling between silicon-on-insulator waveguides and optical fibers," Opt. Lett. **37**, 3483–3485 (2012).
15. L. Chrostowski, J. Flueckiger, C. Lin, M. Hochberg, J. Pond, J. Klein, J. Ferguson, and C. Cone, "Design methodologies for silicon photonic integrated circuits," in *SPIE OPTO* (2014), p. 89890G.
16. J. Pond, C. Cone, L. Chrostowski, J. Klein, J. Flueckiger, A. Liu, D. McGuire, and X. Wang, "A complete design flow for silicon photonics,", in *SPIE Photonics Europe* (2014), pp. 9133–9139.
17. R. J. Bojko, J. Li, L. He, T. Baehr-Jones, M. Hochberg, and Y. Aida, "Electron beam lithography writing strategies for low loss, high confinement silicon optical waveguides," J. Vacuum Sci. Technol. B **29**, 06F309 (2011).

1. Introduction

The silicon-on-insulator platform provides an unprecedented opportunity to make ultra-compact photonic integrated circuits. Due to the large refractive index contrast between the silicon layer and its cladding, propagation modes can be highly confined within the waveguides, with cross-sectional dimensions on the order of a few hundred nanometers. However, the small feature sizes of the waveguide raise the problem of large mode mismatch when coupling light from an optical fiber to the sub-micron silicon waveguide core. Compared with edge couplers, using grating couplers is a popular approach to address the mode mismatch issue and has the advantages of lower cost (e.g., no lensed fibers and no edge polishing), easy-alignment, smaller footprint, etc. Grating couplers also enable wafer-scale automated measurement, without the need to dice the wafer. High-efficiency, shallow-etched grating couplers have been demonstrated [1–3]. Compared with fabrication through Multi Project Wafer (MPW) foundries with long turn-around time and time-consuming design rule checking, rapid prototyping using electron beam lithography with only passive devices provides a low-cost and rapid proof-of-concept alternative. However, for prototyping process using electron beam lithography, fabricating shallow-etched grating couplers more than doubles the process steps and therefore fabrication cost. When combining fundamental building blocks that can be fabricated in a single, fully-etched step, having fully-etched grating couplers provides an efficient and economical solution for rapid prototyping.

R. Halir et al. demonstrated a sub-wavelength grating coupler for the transverse magnetic (TM) mode on the silicon-on-insulator platform [4, 5], and Xu et al. demonstrated a sub-wavelength grating coupler for the transverse electric (TE) mode [6]. However, long adiabatic tapers which consume significant on-chip real-estate were used in their designs to couple the optical modes from the grating to the waveguide. Focusing sub-wavelength grating couplers were demonstrated by Cheng et al. [7] to reduce the footprints of sub-wavelength grating couplers, but special processes and customized wafers were used.

In this paper, we demonstrate fully-etched grating couplers for both the fundamental quasi-TE (TE_{00}) mode and the fundamental quasi-TM (TM_{00}) mode, operating at 1550 nm, with low back reflection and improved coupling efficiency. Our sub-wavelength grating couplers are designed for the silicon-on-insulator wafer with a 220 nm functional silicon layer, which is the same as the wafers provided by the MPW foundry services such as imec, IME, LETI and IHP [1, 8]. Focusing sub-wavelength grating lines have been used to form the effective index region therefore the footprint of the structure can be reduced. Figure 1 shows SEMs of the top

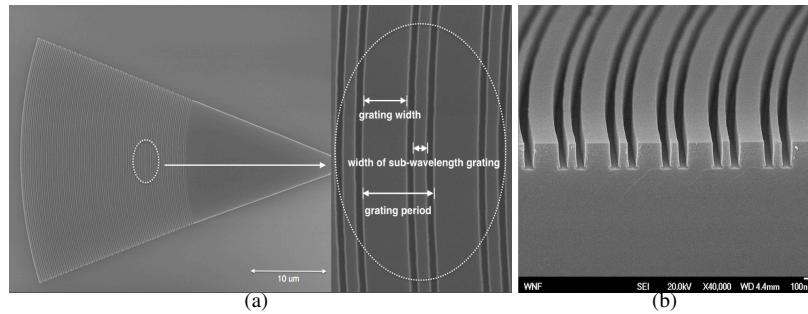view and the sidewall view of our sub-wavelength grating coupler.

Fig. 1. SEM pictures of the focusing sub-wavelength grating coupler. (a) top view; (b) sidewall view.

2. Design and simulation

The critical issues faced by fully-etched grating couplers include high insertion loss and strong back reflection into the waveguide. The high insertion loss is mainly caused by the penetration loss to the substrate and the mode mismatch between the optical fiber and the grating. The large back reflection results from Fresnel reflections caused by the refractive index contrast in the grating region. Diagrams of various types of gratings are shown in Fig. 2. The Fresnel reflection coefficients for the shallow-etched grating and the regular fully-etched grating at 1550 nm are 0.6% and 17%, respectively, which correspond to oscillation ripples with respective extinction ratios of 0.1dB and 3 dB. The refractive index contrast of the regular fully-etched grating is much larger than that of a shallowed-etched grating, which motivates the need for the effective index material to approximate the shallow-etched region in a fully-etched grating coupler. The Fresnel reflection coefficient can be dramatically reduced by using the sub-wavelength grating structure as shown in Fig. 2(c).
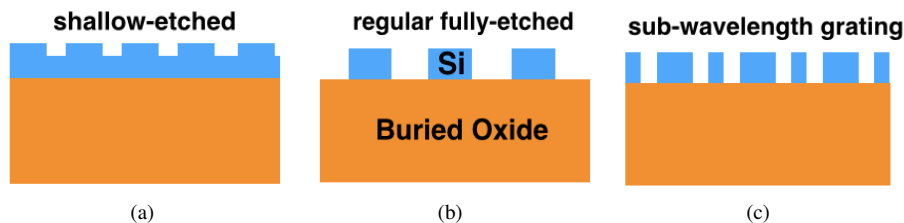

Fig. 2. Cross-section diagrams of various types of gratings (a) shallow-etched grating; (b) regular fully-etched grating; (c) fully-etched sub-wavelength grating.

According to the effective medium theory (EMT), a zeroth-order approximation can be applied to sub-wavelength structures with period-to-wavelength ratios, defined as $R = n_{\text{eff}} \cdot \Lambda/\lambda$, much smaller than 1 [9], where Λ is the period of the structure, λ is the operating wavelength, and n_{eff} is the effective index of the appropriate mode. In previous works, fully-etched squares or quasi-squares were used to form the effective index regions of the grating [5,6,9]. The small dimensions of those sub-wavelength structures are very challenging to fabricate, even with
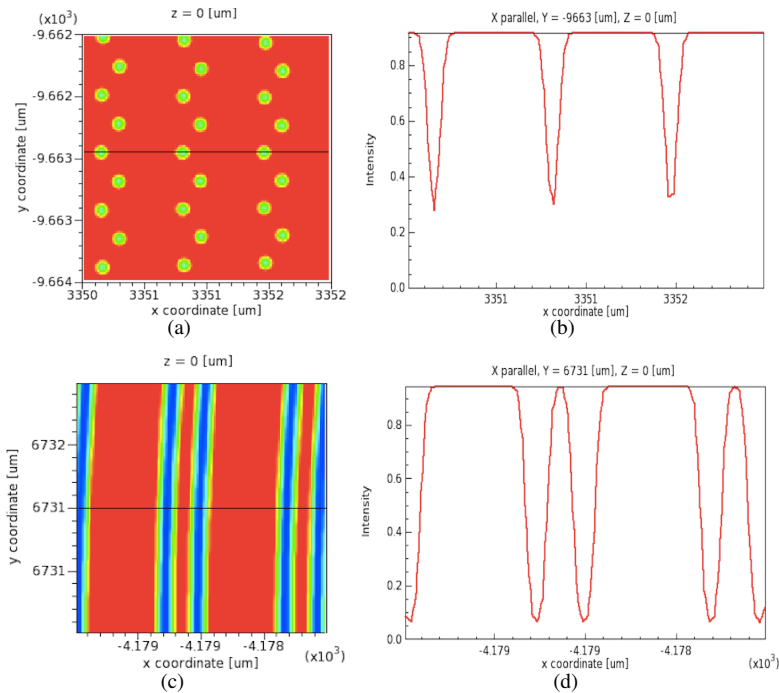
Fig. 3. (a) 2D energy distribution of sub-wavelength grating couplers formed by quasi-squares; (b) energy distribution along the 1-D cutline across the 2-D simulation of sub-wavelength grating coupler formed by quasi-squares; (c) 2D energy distribution of sub-wavelength grating couplers formed by sub-wavelength lines; (d) energy distribution along 1-D cutlines across the 2-D simulations of sub-wavelength grating couplers formed by sub-wavelength grating lines.

high-resolution electron-beam lithography. Sub-wavelength grating lines have been demonstrated in [10] as an alternative to obtain effective index regions, which are easier for fabrication and also enable focusing gratings with smaller footprint using the method demonstrated in [11]. Figure 3 shows the simulated energy distribution from *BEAMER*, a electron-beam lithography software from *GenISys GmbH* [12], for fabricating quasi-squares and sub-wavelength gratings using electron beam lithography. The simulator used a defined Point Spread Function (PSF) for 100 kV electrons on silicon, then produced a 2-D plot of energy distribution after exposure for the pattern data. The PSF shows energy as a function of radial distance from the electron beam, which is caused by electron backscattering and secondary electron generation in the silicon. The lithography simulation applies the PSF to the pattern data, to produce the 2-D energy distribution for different geometries. Figures 3(a) and 3(c) show the respective energy distributions of the quasi-squares and the sub-wavelength grating lines, where the blue denotes the least energy and the red denotes the most energy. The 1-D cutlines across the 2-D simulations show the differences associated with fabricating different type of structures. We get 30% exposure in the quasi-square region as shown in Fig. 3(b) where no exposure is required, whereas for the sub-wavelength grating lines, we only get about 10% exposure as shown in Fig. 3(d) in the region where no exposure is required. Even though high contrast resist process was used, the 30% exposure shown in the quasi-square is still enough energy to at least partially expose the resist, which results in a high variability in feature size. It can be noted that the exposure contrast in the effective index areas has been improved by implementing sub-wavelength grating

lines. As shown in Fig. 1, our sub-wavelength grating coupler consists of two types of gratings: the major (wider) grating and the minor (narrower) grating. The minor gratings are sufficiently small for the optical wave to see the spaces between the major gratings as having an average effective index. For this reason, we call our fully-etched grating coupler a sub-wavelength grating coupler in this paper.

The two-dimensional finite-difference time-domain (FDTD) method was used to optimize the sub-wavelength grating couplers. Three design parameters (the grating period, the grating width, and the width of the sub-wavelength grating as defined in Fig. 1) have been optimized to achieve low insertion loss using the built-in particle swarm algorithm [13] in *FDTD Solutions*, an FDTD-method Maxwell equation solver from *Lumerical Solutions, Inc.*. The light was launched within the waveguide and then diffracted by the grating. A power monitor was positioned on top of the grating to measure the upward power and another mode expansion monitor was used to calculate the coupled power in a specific mode. Eight simulation generations with eight variations within each generation were used to obtain sub-wavelength grating couplers with lowest insertion losses for the TE_{00} mode and the TM_{00} mode. The incident angle of the sub-wavelength grating coupler is determined by the diffraction angle of the grating, which is defined as the angle between the normal of the grating and the diffraction direction of the light wave. The optimized sub-wavelength grating coupler for the TE_{00} mode has a 593 nm grating period, a 237 nm grating width, and a 74 nm sub-wavelength grating. The optimized sub-wavelength grating coupler for the TM_{00} mode has a 960 nm grating period, a 575 nm grating width, and a 140 nm sub-wavelength grating. The incident angles for the sub-wavelength TE and TM grating couplers are -25 degrees and 10 degrees, respectively. A positive incident angle indicates that the diffracted light has a component in the same direction as the incident wave and a negative angle indicates that the diffracted light has a component in the opposite direction as the incident wave.
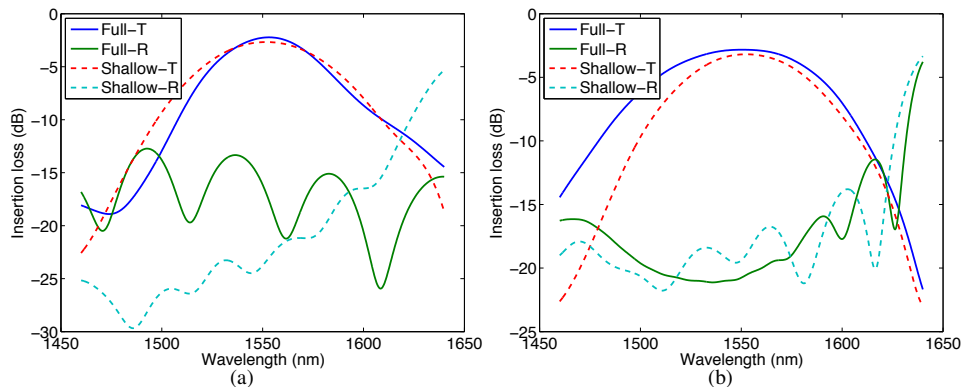

Fig. 4. (a) Simulated transmission and reflection spectra for the optimized sub-wavelength grating coupler and the shallow-etched grating coupler with uniform grating for the TE_{00} mode; (b) simulated transmission and reflection spectra for the optimized sub-wavelength grating coupler and the shallow-etched grating coupler with uniform grating for the TM_{00} mode.

The comparison of the sub-wavelength grating couplers with the shallow-etched grating couplers are shown in Fig. 4. The solid lines denote the transmission and reflection spectra for the sub-wavelength grating couplers and the dashed lines denote the transmission and reflection spectra for the shallow-etched grating couplers. The shallow-etched grating couplers are optimized based on the same wafer type using the same algorithm as the sub-wavelength grating couplers. We can note that our sub-wavelength grating coupler has comparable insertion loss

and reflection near the central wavelength with the shallow-etched grating coupler for the TE_{00} mode. While the sub-wavelength TM grating coupler not only has a lower insertion loss, but also shows a broader bandwidth than the shallow-etched grating coupler. The optimized sub-wavelength grating coupler for the TE_{00} mode shows a simulated insertion loss of 2.2 dB with a 1-dB bandwidth of 32.5 nm (3-dB bandwidth of 58 nm) and the sub-wavelength grating coupler for the TM_{00} mode shows a simulated insertion loss of 2.7 dB with a 1-dB bandwidth of 57 nm (3-dB bandwidth of 92 nm). The optimization was based on uniform gratings, where further improvement can be obtained by apodizing the grating periods to achieve better mode overlap between the grating and the optical fiber. The simulated minimum insertion losses for the apodized sub-wavelength TE and TM grating couplers are 1.6 dB and 1.9 dB, which are comparable to the published state-of-the-art shallow-etched grating coupler [2] without bottom mirrors or top overlays. It should be noted that there are differences in the minimum insertion losses and bandwidths for the sub-wavelength TE and TM grating couplers. The difference in the coupling efficiencies is caused by the different coupling strength of the two grating couplers. The power in the waveguide undergoes an exponentially decay due to the presence of the grating:

$$P_{\text{wg}}(z) = P_{\text{wg}}(z=0) \cdot \exp(-2\alpha z) \tag{1}$$

where 2α is the coupling strength or leakage factor of the grating, $P_{\text{wg}}(z)$ denotes the power of the mode at z, assuming the wave is propagating along the z-axis. The upward diffracted waves by the sub-wavelength TE and TM grating couplers are similar, which are about 69%. However, the coupling strength of the TE and TM grating couplers are different, therefore the coupling losses caused by the mode mismatches between the fiber and grating are different, which lead to the difference in the maximum coupling efficiencies. According to [14], the bandwidth of the grating couplers can be expressed as:

$$\Delta\lambda = \eta_{1\text{dB}}|\frac{d\lambda}{d\theta}| = \eta_{1\text{dB}}|\frac{-\Lambda \cdot n_c \cdot cos(\theta)}{1 - \Lambda \cdot \frac{dn_{\text{eff}}(\lambda)}{d\lambda}}| \tag{2}$$

where $\eta_{1\text{dB}}$ is the 1-dB bandwidth coefficient, Λ is the period of the grating, n_c is the refractive index of the cladding material, n_{eff} is the effective index, and θ is the incident angle. The period of the sub-wavelength TM grating coupler is much larger than that of the TE grating coupler, and the incident angle of the TM grating coupler is smaller than the TE grating coupler, which contribute to a broader bandwidth for the TM grating coupler.
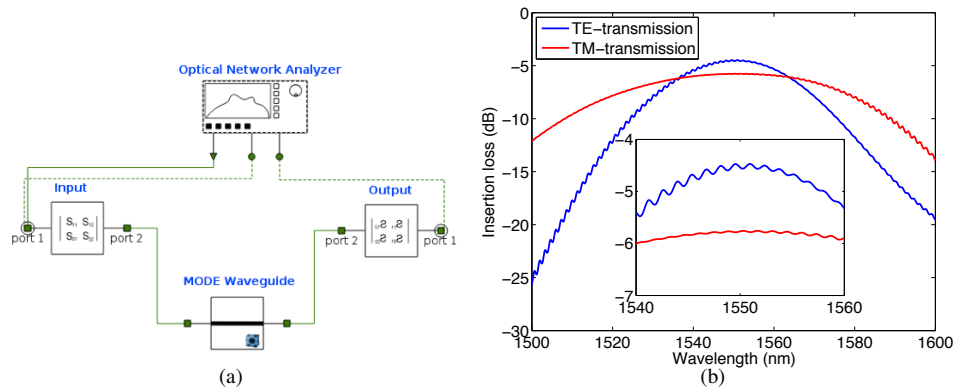

Fig. 5. (a) Schematic of the input-waveguide-output circuit in *Interconnect*; (b) simulated transmission spectra of input-waveguide-ouput circuits for sub-wavelength grating couplers for the TE_{00} (blue line) and TM_{00} (green line) modes.

Figure 4 only shows the simulation results for a single grating coupler, where important features such as oscillation ripples do not occur. In actual photonic circuits, a pair of grating couplers are typically used: one input grating coupler and one output grating coupler. A Fabry-Perot cavity forms between the input and output grating couplers, where the reflected wave propagates between the two gratings and introduces ripples in the spectral responses of the photonic circuits. Scattering parameters (S-parameters) can be used to describe the behaviour of the grating coupler [15]. Simulation of a full input-waveguide-output circuit has been performed using *Interconnect* [16], and Fig. 5(a) shows a schematic of the input-waveguide-output circuit in *Interconnect*. A virtual optical network analyzer is used to generate and measure the optical signal. The grating couplers are represented by two 2-port S-parameter matrices, which were exported from *FDTD Solutions*. The waveguide is a component that can be either loaded from *Interconnect* or imported from *Mode Solutions*, an eigenmode solver from *Lumerical Solutions, Inc.*. The simulated transmission spectra for the input-waveguide-ouput circuits are shown in Fig. 5(b). The blue line shows the simulated transmission spectrum with two sub-wavelength TE grating couplers, with 127 μm pitch, connected by a silicon wire waveguide, and the red line shows the same simulation results for the sub-wavelength TM grating couplers. As shown in Fig. 5(b), the reflections from the sub-wavelength grating couplers have been highly suppressed, and the extinction ratios of the ripples shown for our sub-wavelength TE and TM grating couplers are only 0.3 dB and 0.15 dB, respectively.

3. Fabrication and measurement

Test structures, consisting of an input sub-wavelength grating coupler and an output sub-wavelength grating coupler, with 127 μm pitch, connected by a strip waveguide have been fabricated using electron beam lithography at the University of Washington [17]. The fabrication used silicon-on-insulator wafer with 220 nm thick silicon on 3 μm thick silicon dioxide. The substrates were 25 mm squares diced from 150 mm wafers. After a solvent rinse and hot-plate dehydration bake, hydrogen silsesquioxane resist (HSQ, Dow-Corning XP-1541-006) was spin-coated at 4000 rpm, then hotplate baked at 80 °C for 4 minutes. Electron beam lithography was performed using a JEOL JBX-6300FS system operated at 100 kV energy, 8 nA beam current, and 500 m exposure field size. The machine grid used for shape placement was 1 nm, while the beam stepping grid, the spacing between dwell points during the shape writing, was 6 nm. An exposure dose of 2800 $\mu C/cm^2$ was used. The resist was developed by immersion in 25% tetramethylammonium hydroxide for 4 minutes, followed by a flowing deionized water rinse for 60 s, an isopropanol rinse for 10 s, and then blown dry with nitrogen. The silicon was removed from unexposed areas using inductively coupled plasma etching in an Oxford Plasmalab System 100, with a chlorine gas flow of 20 sccm, pressure of 12 mT, ICP power of 800 W, bias power of 40 W, and a platen temperature of 20 °C, resulting in a bias voltage of 185 V. During etching, chips were mounted on a 100 mm silicon carrier wafer using perfluoropolyether vacuum oil.

Variations have been applied to the grating period, the grating width, and the width of the sub-wavelength grating couplers to understand the sensitivities of various design parameters to the fabrication. Figure 6 shows the central wavelength shifts versus dimension offsets of various design parameters for the sub-wavelength grating coupler. Figure 6(a) is the simulated central wavelength offsets as a function of various design parameter offsets for the sub-wavelength TE grating coupler with an incident angle of -25 degree. The blue circles indicate the central wavelength shift as a function of the grating period offset, the red crosses indicate the central wavelength shift as a function of the grating width offset, and the purple diamonds indicate the central wavelength shift as a function of the width offset of the sub-wavelength grating. Figure 6(b) shows the according measurement results for the sub-wavelength TE grating coupler

with the same incident angle. Same analysis has been applied to the sub-wavelength TM grating couplers and the results are shown in Fig. 6(c) and Fig. 6(d) except that the incident angle was 10 degrees for the sub-wavelength TM grating couplers. The measurement data points shown in Fig. 6 are extracted from the measurement spectra shown in Figs. 8(d)–8(f). Linear-fits have been applied to compare the sensitivities of various design parameters (grating period, grating width, and the width of the sub-wavelength grating) and the corresponding slopes are shown in Table 1. It can be noted that the slopes calculated from the experimental results are slightly smaller than the simulated results for both the TE and the TM grating couplers, but the comparative relation between those values are the same in both cases. The width of the sub-wavelength grating and the grating period are the key parameters affecting the central wavelength of the sub-wavelength TE and TM grating couplers, respectively. In addition, we can notice that the slopes of various design parameters for the TM grating coupler are smaller than that of the TE grating coupler, which indicate a lower sensitivity to fabrication variations/errors.
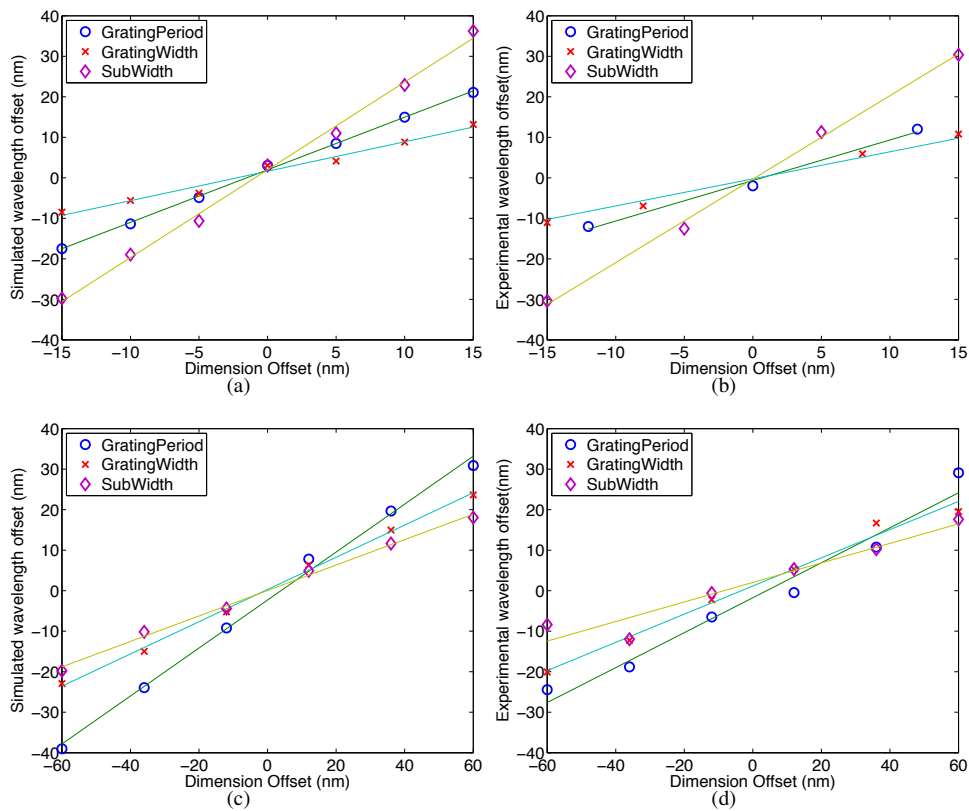

Fig. 6. (a) Simulated sensitivities of the grating period, the grating width, and the sub-wavelength grating for the sub-wavelength TE grating coupler; (b) Measured sensitivities for the sub-wavelength TE grating coupler; (c) Simulated sensitivities for the sub-wavelength TM grating coupler; (d) Measured sensitivities for the sub-wavelength TM grating coupler.

The comparison of the simulated and measured transmission spectra for the optimized sub-wavelength TE grating coupler are shown in Fig. 7. The back reflection from our sub-wavelength grating coupler has been highly eliminated by using the effective index material hence the ripples in our transmission spectrum caused by the Fabry-Perot cavity are signifi-

Table 1. Simulated and measured sensitivities of the central wavelength offset to various design parameters

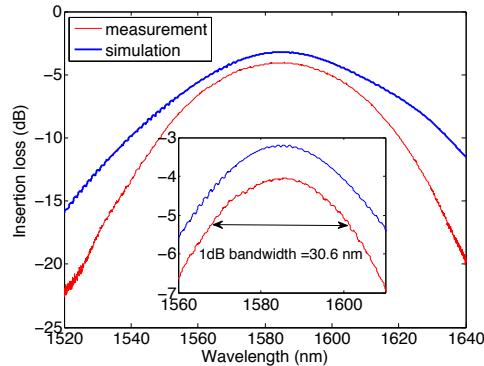|	TE		TM	
	simulation (nm/nm)	experiment (nm/nm)	simulation (nm/nm)	experiment (nm/nm)
Grating period	1.3	1.0	0.59	0.43
Grating width	0.73	0.67	0.39	0.35
Sub-wavelength grating	2.1	2.06	0.31	0.24

Fig. 7. Simulated and measured transmission spectra of the fabricated sub-wavelength TE grating coupler assuming the width of the sub-wavelength grating is 89 nm; inset is the spectrum near the central wavelength.

cantly suppressed (< 0.25 dB), which is comparable to that of a shallow-etched grating coupler (about 0.1 dB). The free spectral range of the ripples near the central wavelength is about 1.6 nm, which correspond to a cavity length of 189 μm, assuming only waveguide, with a group index of 4.33, exists between the input and output fibers. The total waveguide length between the input and output grating couplers is 183 μm, which means the air gap between the fiber tip and the chip surface, with a group index of 1, is about 25 μm during our measurement. Due to fabrication inaccuracies, the measured central wavelength shifted to 1580 nm. As shown in Table 1, the slope of the sub-wavelength grating is much larger than that of the grating period and the grating width. In addition, the feature size of the sub-wavelength grating (74 nm) is much smaller than the grating period (593 nm) and the grating width (237 nm). The red shift of the spectrum is mainly caused by the fabrication inaccuracy in the sub-wavelength grating, though it may also be caused by the fabrication inaccuracies in the grating period and the grating width. The simulation results shown in Fig. 7 assumed that the central wavelength shift was caused by the fabrication offset in the sub-wavelength gratings, and a 15 nm offset was assumed when the simulated central wavelength matches the measurement results. There are also mismatches of insertion loss and bandwidth between the simulated and measured results, which are mainly caused by the fiber array we used. We intentionally polished our fiber array with a large angle so that it can accommodate for various incident angles. The actual incident angle for the sub-wavelength TE and TM grating couplers are smaller than the polished angle, so the chip surface and the fiber tip were not parallel during the measurement. Therefore an inevitable gap was introduced between the fiber tip and measured chip, which leads to a higher insertion loss and a smaller bandwidth. In addition, extra insertion losses were also introduced from the transmission lines (optical fibbers) and the interfaces of the connectors used in the
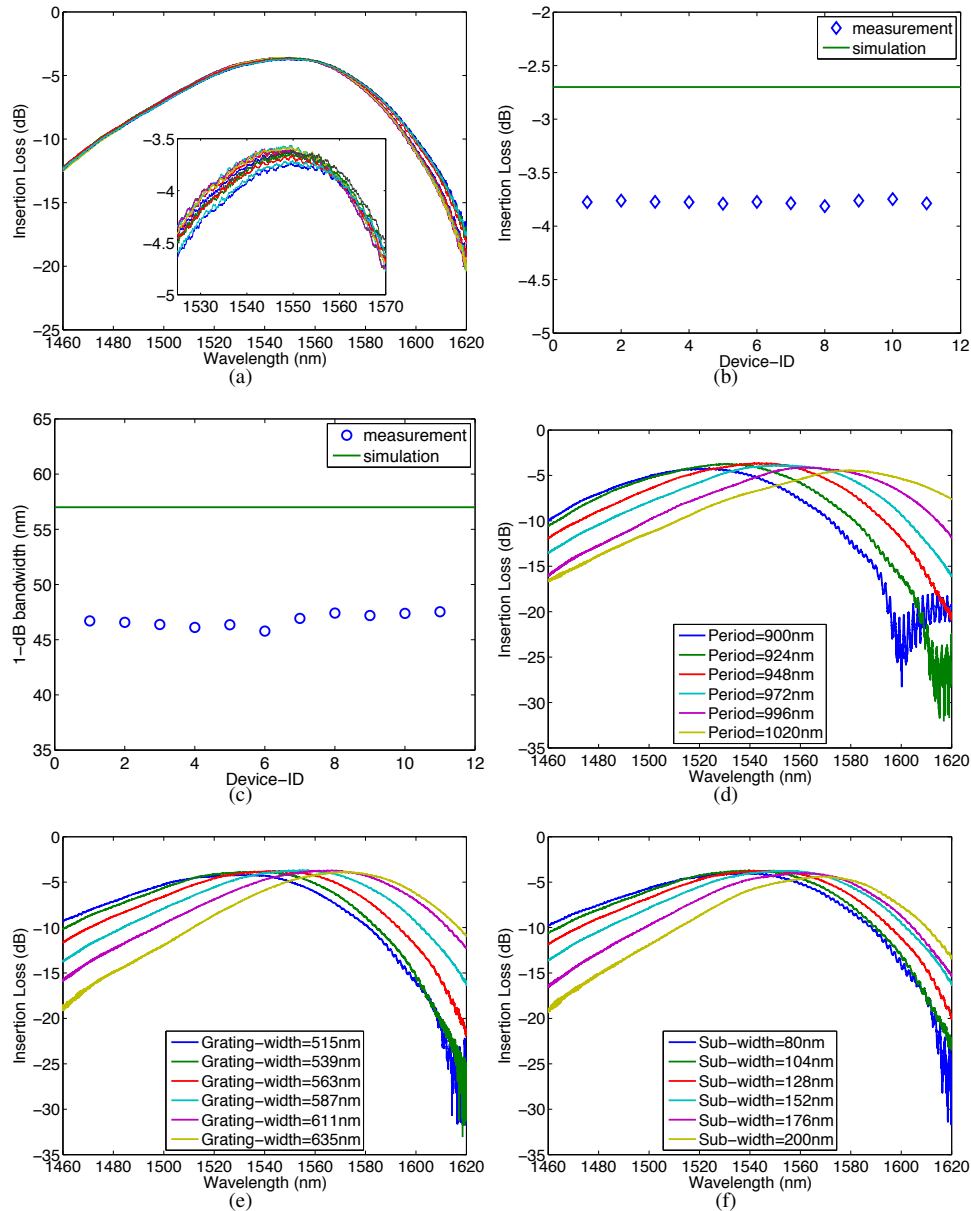
Fig. 8. (a) Measured spectra of 11 standard sub-wavelength TM grating couplers; (b) comparison of measured insertion losses of the 11 standard sub-wavelength TM grating couplers and the simulated insertion loss; (c) comparison of the measured 1-dB bandwidths of the 11 standard sub-wavelength TM grating couplers and the simulated 1-dB bandwidth; (d) measured spectra of sub-wavelength TM grating couplers with various grating widths; (e) measured spectra of sub-wavelength TM grating couplers with various grating periods; (f) measured spectra of sub-wavelength TM grating couplers with various widths of sub-wavelength grating.

measurement system, which have not been calibrated out from the measurement results.
The measurement results for the sub-wavelength TM grating couplers are shown in Fig. 8.

Figure 8(a) shows the measured spectra of 11 standard sub-wavelength TM grating couplers with the same design parameters. The inset of the graph shows the zoomed spectra near the central wavelength. Figures 8(b) and 8(c) show the comparison of the measured insertion losses and 1-dB bandwidths of the 11 standard sub-wavelength TM grating couplers with the simulated results. The green lines denote the simulation results and the blue diamonds and circles denote the measurement results extracted from the spectra shown in Fig. 8(a). The insertion losses of the 11 sub-wavelength TM grating couplers range from 3.7 dB to 3.8 dB with the 1-dB bandwidth ranging from 45.8 nm to 47.5, nm, which shows good performance stability and device repeatability. The best device has an insertion loss of 3.7 dB with a 1-dB bandwidth of 47.5 nm. Figures 8(d)–8(f) show the measured spectra of sub-wavelength TM grating couplers with various grating periods, grating widths and sub-wavelength gratings. The offsets versus central wavelength shifts of those design parameters have been shown in Fig. 6 and the linear-fits of those design parameters have been given in Table 1. The central wavelengths of the sub-wavelength TM grating couplers are proportional to the grating period, the grating width and the width of the sub-wavelength grating. The sub-wavelength TM grating couplers did not have a large central wavelength shift as the sub-wavelength TE grating coupler did for two reasons. The first reason is that the feature size of the sub-wavelength TM grating coupler is much larger than the TE grating coupler, which makes it less challenging for the fabrication process. The second reason is that, according to the linear-fits shown in Table 1, the central wavelength of the TM grating coupler is less sensitive to the offsets of various design parameter, which is caused by the weak confinement of the TM mode.

4. Conclusion

We have demonstrated compact sub-wavelength grating couplers for both TE and TM modes. The back reflections from our sub-wavelength grating couplers have been significantly suppressed compared to the regular fully-etched grating couplers. It has also been shown by the simulation and experimental results that the sub-wavelength grating line is an alternative to the quasi-squares to achieve effective index region with better fabrication accuracy and less complexity. Our sub-wavelength TE grating coupler with uniform gratings has a measured insertion loss of 4.1 dB with a 1-dB bandwidth of 30.6 nm (3-dB bandwidth of 52.3 nm) and the sub-wavelength TM grating coupler has a measured insertion loss of 3.7 dB with a 1-dB bandwidth of 47.5 nm (3-dB bandwidth of 81.5 nm). Further improvement can be made by apodizing the grating periods and the simulated minimum insertion losses of our sub-wavelength TE and TM grating couplers are comparable to the published state-of-the-art shallow-etched grating couplers. As the resolution of the CMOS fabrication becomes smaller, those fully-etched sub-wavelength grating couplers can even become alternatives to the shallow-etched grating couplers therefore the fabrication cost and complexity can be reduced.